JOURNAL OF APPLIED ELECTROCHEMISTRY **26** (1996) 603–611

Determination of transport and electrochemical kinetic parameters of M–H electrodes

B. N. POPOV, G. ZHENG, R. E. WHITE

Department of Chemical Engineering, University of South Carolina, Columbia, SC 29210, USA

Received 6 June 1995; revised 20 November 1995

Electrochemical and transport properties of $La_{0.65}Ce_{0.35}Ni_{3.55}Co_{0.75}Mn_{0.4}Al_{0.3}$ electrode were investigated in alkaline solution. The exchange current density, polarization resistance and the symmetry factor were determined from polarization curves obtained at low overpotentials. The symmetry factor was estimated to be 0.55 ± 0.01 and is independent of the state of charge. The equilibrium potential of the electrode was found to depend upon the hydrogen content in the alloy. The constant current discharge technique was used to determine the hydrogen diffusion coefficient in the alloy. The estimated value of $\bar{D}/a^2$ at 0.1 C discharge rate was $1.39 \times 10^{-4}\,s^{-1}$.

List of symbols

a	sphere radius (cm)
a_i	relative activity for species i (mol cm^{-3})
A_s	the exposed surface area of the electrode (cm^2)
c_H	hydrogen content (atoms cm^{-3})
C_{H_2O}	concentration of H_2O (mol cm^{-3})
C_{OH^-}	concentration of OH^{-1} (mol cm^{-3})
D_i	the effective diffusion coefficient (cm^2 s^{-1})
$\bar{D}$	integral diffusion coefficient of hydrogen (cm^2 s^{-1})
E_{eq}	equilibrium potential (V)
E^0	standard potential (V)
e^-	electronic charge (C)
F	Faraday's constant (96 487 C equiv.$^{-1}$)
I	current (A)
i	current density per unit of mass (A g^{-1})
i_s	current density (A cm^{-2})
i_0	exchange current density per unit of mass (A g^{-1})
j'	microkinetic current density (A cm^{-2})
j'_0	exchange current density per unit of electroactive area (A cm^{-2})
f	frequency (Hz)
K	constant defined by Equation 6 (dimensionless)
L	half thickness of electrode (cm)
M	the total mass of the electrode (g)
m	OH^- reaction order (dimensionless)
n	hydrogen reaction order (dimensionless)
p	H_2O reaction order (dimensionless)
Q_0	the initial charge in the electrode (C g^{-1})
Q_1	charge remaining in the electrode after discharge (C g^{-1})
r	distance from the centre of a spherical particle (cm)
R	gas constant (8.314 J mol^{-1} K^{-1})
R_e	electrolyte resistivity (Ω cm)
R_p	polarization resistance (Ω g)
T	temperature (K)
t	time (s)
t_{ch}	charging time (s)
x	distance from the pellet surface (cm)
v	sweep rate (V s^{-1})

Greek symbols

β	symmetry factor (dimensionless)
γ	activity coefficient (dimensionless)
ϵ	electrode porosity (dimensionless)
η	overpotential (V)
ρ	density (g cm^{-3})
τ	transition time (s)
τ_t	tortuosity (dimensionless)

Subscripts

b	bulk of the electrolyte
i	electrolyte/electrode interface
p	pores of the electrode

1. Introduction

The electrochemical kinetic properties and transport properties of M–H electrodes such as the polarization resistance, the exchange current density, the symmetry factor and the hydrogen diffusion coefficient are important parameters which characterize the performance of the electrode [1–6]. According to Wiswall [7], the maximum hydrogen content in the alloy is of the same order of magnitude as the host metal atoms. Yayama *et al.* [8] determined the dependence of the exchange current density of $TiMn_{1.5}H_x$ (<0.31) as a function of the hydrogen content in the alloy. Noten and Hokkeling [9] derived a similar concentration gradient expression for exchange current density including in the expression the influence of electrode blocking on exchange current density by chemically adsorbed species involved in the electrochemical reaction. Austin [10, 11] derived a general equation for potential–time relationship for porous, flooded

0021-891X © 1996 Chapman & Hall

diffusion electrode taking into account both the mass transport and the ohmic effects.

In the present study the transport and electrochemical properties of $La_{0.65}Ce_{0.35}Ni_{3.55}Co_{0.75}Mn_{0.4}Al_{0.3}$ electrode were investigated in alkaline solution. The exchange current density, polarization resistance and symmetry factor were determined from the polarization curves obtained at low overpotentials using porous electrode theory. According to Sakai *et al.* [12, 13] Ce, Nd and Pr substitutions at the A site in AB_5 hydride electrodes resulted in improved capacity retention during cycling. Adzic *et al.* [14] studied the effect of increasing Ce content upon electrode cycle life of $La_{1-x}Ce_x Ni_{3.55}Co_{0.75}Mn_{0.4}Al_{0.3}$. It was found that the rate of loss of electrochemical capacity per charge/discharge cycle was significantly decreased due to presence of Ce in the alloy. Thus, $La_{1-x}Ce_xNi_{3.55}Co_{0.75}Mn_{0.4}Al_{0.3}$ alloys appear to be promising hydrogen absorbing alloys because of their resistance to degradation.

2. Theory

The main electrode reactions occurring at metal hydride electrode are as follows:

$$M + H_2O + e^- \rightleftharpoons MH_{ads} + OH^- \quad (1)$$

$$MH_{ads} \rightleftharpoons MH_{abs} \quad (2)$$

and

$$MH_{abs} \rightleftharpoons MH_{hyd} \quad (3)$$

where H_{ads}, H_{abs}, and H_{hyd} represent the hydrogen atom adsorbed on the surface, absorbed in the electrode and hydride, respectively. The microkinetic current density (j'), that is, the current per unit of electroactive surface area of the electrode from Equation 1, can be written as [10]

$$j' = j'_0\left[-\frac{C_{H_2O(p)}}{C_{H_2O(b)}}\exp\left(\frac{-\beta F}{RT}\eta\right) + \frac{C_{OH^-(p)}}{C_{OH^-(b)}}\exp\left(\frac{(1-\beta)F}{RT}\eta\right)\right] \quad (4)$$

where j'_0 is exchange current density, C_i's are the concentration for species i, β is the symmetry factor, F is the Faraday constant, R is the gas constant, T is the temperature, and η is the overpotential. Subscripts 'p' and 'b' represent the 'pore' of the electrode and 'bulk' of the electrolyte, respectively.

According to Austin [10, 11], assuming that (i) the mass transfer factors of H_2O and OH^- are the same so that $C_{H_2O(p)} + C_{OH^-(p)} = C_{H_2O(b)} + C_{OH^-(b)}$ and (ii) the potential drop through the pore electrolyte is sufficiently small so that the overpotential is a constant η, one may obtain the following expression for current density [10, 11]

$$i = i_0\left[-\frac{C_{H_2O(i)}}{C_{H_2O(b)}}\exp\left(\frac{-\beta F}{RT}\eta\right) + \frac{C_{OH^-(i)}}{C_{OH^-(b)}}\exp\left(\frac{(1-\beta)F}{RT}\eta\right)\right]\frac{\tanh(\sqrt{K})}{\sqrt{K}} \quad (5)$$

and

$$K = \frac{i_0 LM}{A_s F D_{H_2O}} \times\left\{\frac{\exp[-\beta F\eta/RT]}{C_{H_2O(b)}} + \frac{\exp[-(1-\beta)F\eta/RT]}{C_{OH^-(b)}}\right\} \quad (6)$$

Note, for convenience, the current density per unit of electroactive surface area (j') in Equation 6 is expressed in terms of current density per unit mass (i). A_s is the cross-sectional area of the electrode, L is the half-thickness of the electrode, M is the total mass of the electrode, D_{H_2O} is the effective diffusion coefficient of water.

If i_0L and the electrode polarization overpotential are low, then $\sqrt{K}$ is small so that $\tanh(\sqrt{K})/\sqrt{K} \approx 1$ and the external concentration drops are negligible, then Equation 5 reduces to

$$i = i_0\left[-\exp\left(\frac{-\beta F}{RT}\eta\right) + \exp\left(\frac{(1-\beta)F}{RT}\eta\right)\right] \quad (7)$$

which is a conventional equation for plane electrode, however, it may only be applied for low overpotential. Further, Equation 7 may be linearized as

$$i = i_0\frac{F\eta}{RT} \quad (8)$$

and the equation for polarization resistance (R_p) may be written as

$$R_p = \frac{RT}{Fi_0} \quad (9)$$

Therefore, the exchange current density and polarization resistance may be determined from the linear polarization curves by using Equations 8 and 9, respectively. However, the symmetry factor (β) cannot be determined from conventional Tafel since the normal Tafel equation does not apply for the porous electrodes [10, 11, 20]. To evaluate the symmetry factor, Equation 7 may be rewritten as

$$\frac{i}{\exp(F\eta/RT) - 1} = i_0\exp\left(\frac{-\beta F\eta}{RT}\right) \quad (10)$$

Taking logarithm of Equation 10, one obtains [15, 16]

$$\eta = \frac{2.3RT}{\beta F}\log i_0 - \frac{2.3RT}{\beta F}\log\left[\frac{i}{\exp(F\eta/RT) - 1}\right] \quad (11)$$

Thus, from the slope of the plot of η against $\log i/[\exp(F\eta/RT) - 1]$, the symmetry factor can be determined. Equation 11 is only valid in the low overpotential region [20].

3. Experimental details

3.1. *Preparation of metal hydride electrodes*

The alloy $La_{0.65}Ce_{0.35}Ni_{3.55}Co_{0.75}Mn_{0.4}Al_{0.3}$ powder obtained from Brookhaven National Laboratory was passed through a 230 mesh sieve, which gave a particle size of less than 60 μm. Next, pellet electrodes

were prepared by mixing the alloy powder with 2.5 wt% (w/o) PTFE followed by pressing the material between two platinum meshes in a cylindrical press. A pellet with a diameter of 0.8 cm and weight of 115 mg was formed at approximately 300 °C using a pressure of 5 torr cm^{-2}. A good electrical connection to the pellet was achieved through the following procedure: (i) a piece of platinum wire was passed several times through a platinum mesh; (ii) the platinum mesh and the wire were then pressed together to obtain good electrical contact. The pellet was then inserted between two pieces of plexiglass holder with small holes on each side and immersed in the test cell filled with a 6 M KOH electrolyte solution. A piece of Pt gauze on each side of the electrode served as a counter electrodes. The experiments were carried out using the SoftCorr System (model 342C) with a EG&G Princeton Applied Research potentiostat/galvanostat (model 273A) at 25 °C.

3.2. *Experimental procedure*

The experimental procedure was performed as follows: after activation (by repeating charge/discharge cycles) the electrode was charged under a constant current mode until the hydrogen content reached its saturated value. The equilibrium potential was measured against the Hg/HgO reference electrode. Next, linear polarization and a.c. impedance experiments were carried out. The measurements were performed only after the open circuit potential was stabilized (i.e., the change of the potential was less than 1 mV for a period of 1 h). The electrode was discharged for a certain period of time and the same measurements as above were conducted. This procedure was repeated until the electrode was discharged to the potential of −0.6 V vs Hg/HgO reference electrode.

4. Results and discussion

4.1. *Discharge characteristics*

Discharge curves for $La_{0.65}Ce_{0.35}Ni_{3.55}Co_{0.75}Mn_{0.4}Al_{0.3}$ alloy using 0.1 C rate ($i = 27.8\,mA\,g^{-1}$), 0.2 C rate ($i = 55.6\,mA\,g^{-1}$) and 0.5 C rate ($i = 139\,mA\,g^{-1}$) in 6 M KOH are shown in Fig. 1. Assuming that six hydrogen atoms are adsorbed by one formula of the alloy, the theoretical capacity was calculated to be 381 mA h g^{-1}. The experimental capacity of the $La_{0.65}Ce_{0.35}Ni_{3.55}Co_{0.75}Mn_{0.4}Al_{0.3}$ alloy is 278 mA h g^{-1} which is about 73% of the theoretical capacity. Adzic *et al.* [14] investigated the alloys of $La_{1-x}Ce_xNi_{3.55}Co_{0.75}Mn_{0.4}Al_{0.3}$ and found the maximum capacity of 84, 276 and 340 mA h g^{-1} for Ce content in the alloy of $x = 0.75$, 0.5 and 0.2, respectively. As shown in Fig. 1 as the discharge rate increases, the state of discharge at the end of discharge (cutoff voltage = −0.6 V vs Hg/HgO reference electrode) decreases. The observed decrease of the state of charge is due to the depletion of atomic hydrogen from the surface of the MH particles at high discharge rates. This phenomena causes the potential to drop before all the hydrogen contained in the particles has been reacted.

4.2. *Electrochemical determination of hydrogen diffusion coefficient through the electrode*

Assuming that the hydride alloy particles are in spherical form, the diffusion equation is

$$\frac{\partial(rc)}{\partial t} = \bar{D}\frac{\partial^2(rc)}{\partial r^2} \tag{12}$$

where c is hydrogen concentration in the alloy, t is time, $\bar{D}$ is an average (or integral) diffusion coefficient of hydrogen over a defined concentration range and r

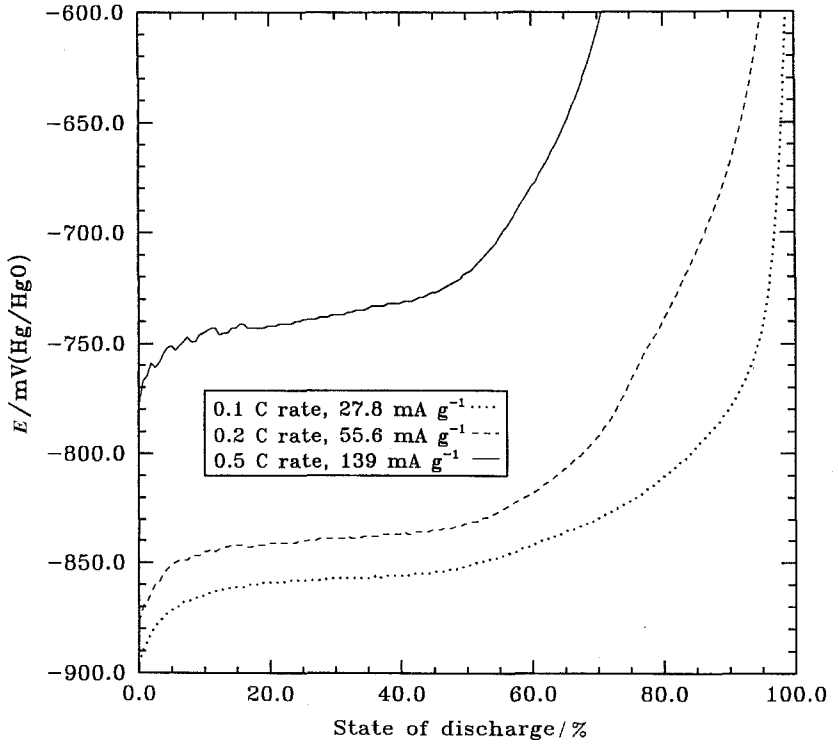

Fig. 1. Dependence of E on state of discharge. Discharge rates: (——) 0.5 C, 139 mA g^{-1}; (– – –) 0.2 C, 55.6 mA g^{-1}; (· · · ·) 0.1 C, 27.8 mA g^{-1}.

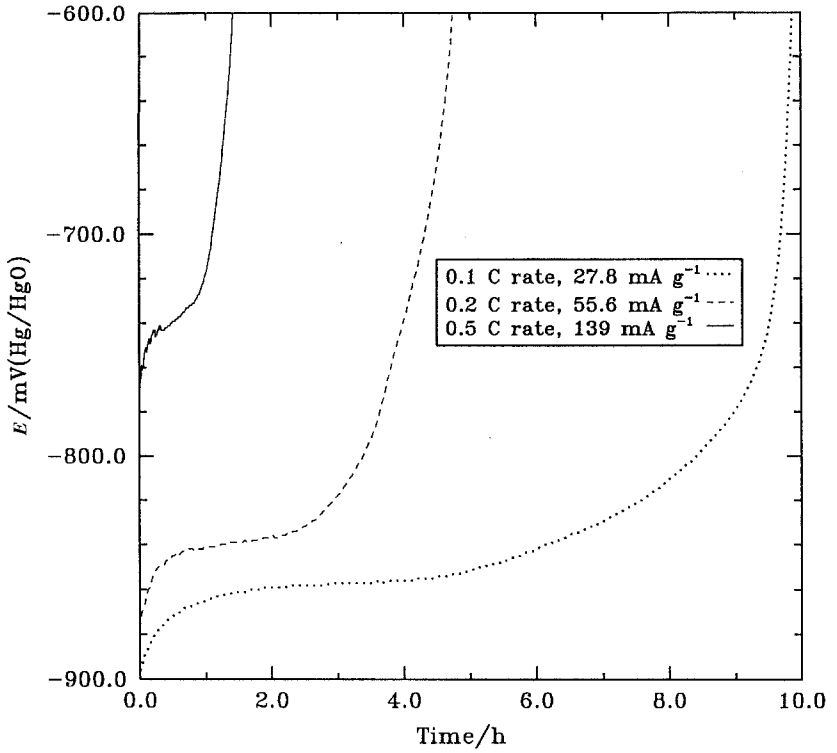

Fig. 2. Dependence of E on time. Discharge rates: (——) 0.5 C, 139 mA g^{-1}; (– – –) 0.2 C, 55.6 mA g^{-1}; 0.1 C, 27.8 mA g^{-1}

is a distance from the centre of the sphere. The diffusion equation may be solved under two different boundary conditions: (i) constant hydrogen surface concentration and uniform initial hydrogen concentration in the bulk alloy, and (ii) constant flux at the surface and uniform initial concentration in the bulk of the alloy. Assuming constant flux at the surface and uniform initial concentration of hydrogen in the bulk of the alloy, the value of $\bar{D}/a^2$ may be evaluated for large transitions times, τ [17, 18]:

$$\frac{\bar{D}}{a^2} = \frac{1}{15}\left(\frac{Q_0}{i} - \tau\right)^{-1} \tag{13}$$

where a is the alloy particle radius, Q_0 is the initial specific capacity (C g^{-1}) and i is the discharge current density (A g^{-1}) and τ is the transient time (s), that is, the time required for the hydrogen surface concentration to become zero. The ratio Q_0/i corresponds to the discharge time necessary to completely discharge the electrode under hypothetical conditions when the process proceeds without interference of diffusion. Rearranging Equation 13, gives

$$Q_1 = Q_0 - \tau i = \frac{i}{15}\frac{a^2}{\bar{D}} \tag{14}$$

where Q_1 is charge of hydrogen left in the electrode when the hydrogen surface concentration is zero. According to Equation 14, the hydrogen content left over in the electrode after discharge is proportional to the discharge current and to the square of particle size and is inversely proportional to the diffusion coefficient.

The galvanostatic discharge curves presented in Fig. 1 were replotted in Fig. 2 in real time. The discharge experiments were terminated at a potential of −0.6 V vs Hg/HgO. To evaluate the diffusion coefficient using Equation 13 it is necessary to estimate the transition time τ. As shown in Fig. 2, after a certain period of time, a drastic potential change occurred to compensate the hydrogen surface concentration decreasing in order to keep a constant current. The terminated times in Fig. 2 were taken as the transition times. Thus, the knee in the discharge curve was assumed to be caused by depletion of hydrogen atoms at the surface of the electrode. However, one may speculate that the knee in the potential–time curves may also occur due to the porous nature of the electrode. In other words due to pore resistance, the reaction rate is higher at the surface of the electrode causing faster depletion which will result in a potential change in the polarization curve. However, the local hydrogen depletion would be possible only if the potential drop due to the pore resistance is significant. The potential drop due to the pore resistance may be expressed as

$$\Delta\eta = i_s \frac{\tau_t R_e}{\epsilon} x \tag{15}$$

where $\Delta\eta$ is the potential drop, i_s is the current density (A cm^{-2}), R_e is the electrolyte resistivity ($R_e = 1.56\,\Omega$ cm for 6 M KOH [21], ϵ is the electrode porosity (0.4) which was calculated from the total mass, pillet thickness and the alloy and binder densities, τ_t is the tortuosity ($\tau_t = 2$) and x is the distance from the pellet surface (cm). The discharge current density was $i = 27.8$ mA g^{-1} (approximately 0.1 mA cm^{-2}). Taking into account that current collectors are on each side of the pellet, one may estimate the potential drop by substituting the half thickness of the pellet into Equation 15, which gives

$$\Delta\eta = \left(0.1\frac{\text{mA}}{\text{cm}^2}\right)\left(\frac{2 \times 1.56\,\Omega\,\text{cm}}{0.4}\right)\left(\frac{0.055\,\text{cm}}{2}\right)$$
$$= 0.02\,\text{mV} \tag{16}$$

Thus, the maximum potential drop due to the pore resistance from the electrode interface to the centre of the pellet is about 0.02 mV, which is negligible and indicates that local hydrogen depletion is not possible.

The estimated transition times were 35 520 s, 17 100 s and 5 092 s, respectively. The initial charge in the electrode, Q_0 was 1008 C g^{-1}, (278 mA h g^{-1}). Thus, the calculated values of $\bar{D}/a^2$ using Equation 13 were: $1.39 \times 10^{-4}\ s^{-1}$, 7.41×10^{-5} s, and $3.16 \times 10^{-5}\ s^{-1}$, respectively. The value calculated from the curve obtained at 0.1 *C* rate is closer to the actual value of $\bar{D}/a^2$ because of the following facts: (i) Equation 13 is valid for large transition times [17, 18] and (ii) since the time at the cutoff potential (−0.6 V vs Hg/HgO) was taken as transition time, it is not correct to assume that at this time the hydrogen concentration on the surface will reach a value which is close to zero for each of the above discharge rates. This can be seen clearly from Fig. 1. The curve obtained at discharge rate of 0.1 *C* rate shows steeper slope than the other two curves, which indicates that at cutoff time, the hydrogen concentration on the electrode at this rate was closer to zero than at the other two discharge rates. The charges remaining in the electrode after discharge for τ seconds were estimated to be 293 C g^{-1}, 50 C g^{-1} and 13 C g^{-1} for discharge rates of 0.5 *C* rate, 0.2 *C* rate and 0.1 *C* rate, respectively.

4.3. *Dependence of equilibrium potential on state of charge*

The equilibrium potentials (E_e) as a function of state of charge in the electrode is presented in Fig. 3. The state of charge is defined as a ratio between the amount of charge in the electrode and measured maximum possible charge in the electrode. As shown in this Figure, two phases exist in the alloy. When the state of charge of the electrode is less than 25%, the equilibrium potential of the electrode changes rapidly with the hydrogen content in the alloy. This region, so-called α phase, or a solid solution phase [19]. According to Yayama [8], the metal hydride electrode equilibrium potential depends upon the hydrogen content in the electrode according to

$$E_e = E'_0 - n\frac{RT}{F}\{\ln\gamma + \ln c_H\} \qquad (17)$$

where γ is the activity coefficient of hydrogen, n is hydrogen reaction order and $E'_0 = E^0 + (RT/F)\ln(a^p_{H_2O}/a^m_{OH^-})$. Although the activity coefficient is unknown, it is reasonable to assume that γ approaches unity in the limiting case when the hydrogen content approaches zero. Thus, Equation 17 may be applicable only at very low hydrogen content in the alloy (i.e., in the α phase). The concentration of hydrogen atoms, c_H, can be calculated by using Faraday's law if the amount of charged supplied during the charge period is known:

$$c_H(\text{atoms cm}^{-3}) = I(\text{A})t_{ch}(\text{s})\rho(\text{g cm}^{-3})/e^-(\text{C}) \quad (18)$$

where e^- is the electronic charge and t_{ch} is the charging time. The equilibrium potential measured as a function of state of charge in Fig. 3 agrees qualitatively at low state of charge with the predictions of Equation 17. Equation 17 includes E'_0 which is affected by changes in the structure of the double layer and surface specific chemisorption and γ which is not constant (and is not equal to unity at higher state of charges). Thus, both parameters may contribute for the observed qualitative relationship in Fig. 3.

Increasing the hydrogen content in the electrode, the equilibrium potential as shown in Fig. 3 reaches a plateau. At this region, two phases α and β (hydride

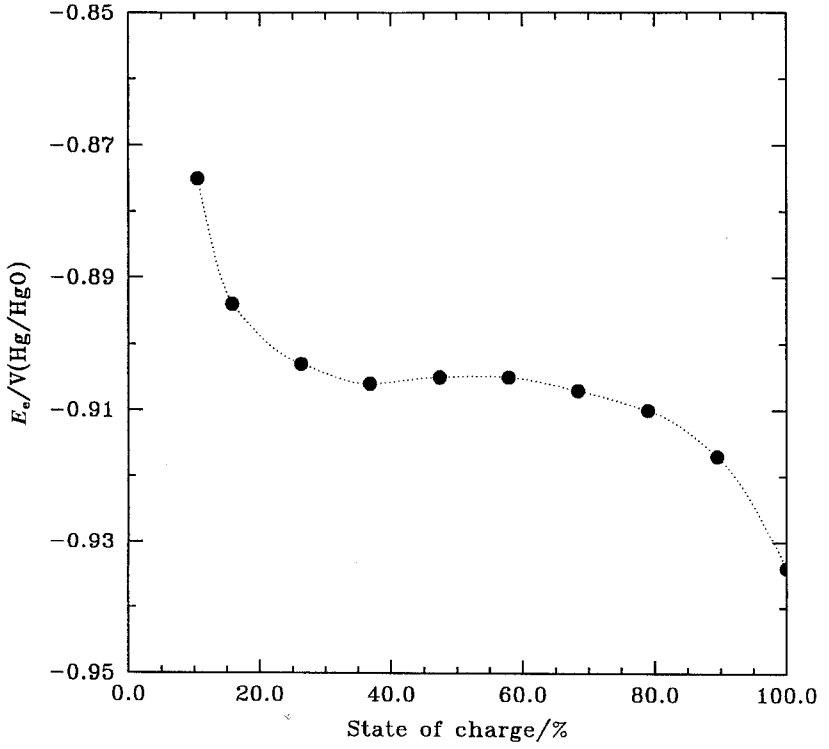

Fig. 3. Equilibrium potential of the electrode as a function of state of charge.

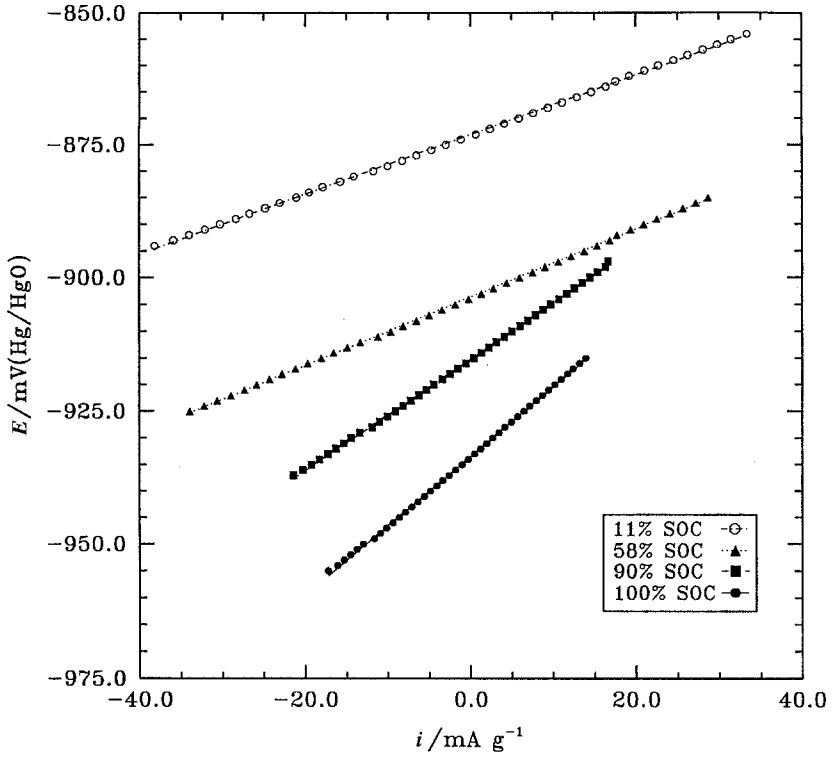

Fig. 4. Typical linear polarization curves of the electrode. Scan rate: 10 mV s^{-1}. States of charge: (●) 100%, (■) 90%, (▲) 58% and (○) 11%.

phase) coexist. When only β phase exists in the alloy (at about 80% state of charge), the equilibrium potential starts to increase again with the increase of hydrogen content in the alloy and at 100% state of charge reaches a value of −0.934 V vs Hg/HgO reference electrode.

4.4. *Linear polarization studies*

The potential loss of the electrode according to Equation 8 is due to the charge transfer overvoltage and increases with current density. Accordingly, the exchange current density should be as large as possible to reduce the charge transfer overvoltage and the corresponding potential loss. Thus, estimation of exchange current density gives information about the performance of the electrode material. According to our previous studies [20], conventional Tafel polarization method cannot be applied to estimate the exchange current density for porous metal hydride system due to presence of internal mass transfer effects and internal ohmic drop of the electrode. Thus, in the present study, both the exchange current density and symmetry factor of $La_{0.65}Ce_{0.35}Ni_{3.55}Co_{0.75}Mn_{0.4}Al_{0.3}$ alloy were evaluated from polarization curves obtained at low overpotentials.

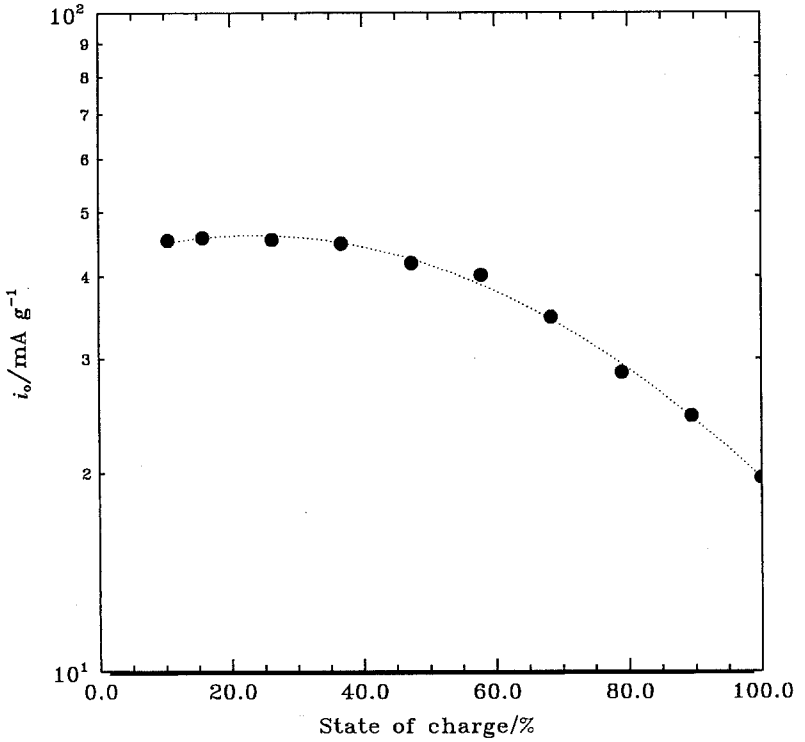

Fig. 5. Exchange current density of the electrode as a function of state of charge.

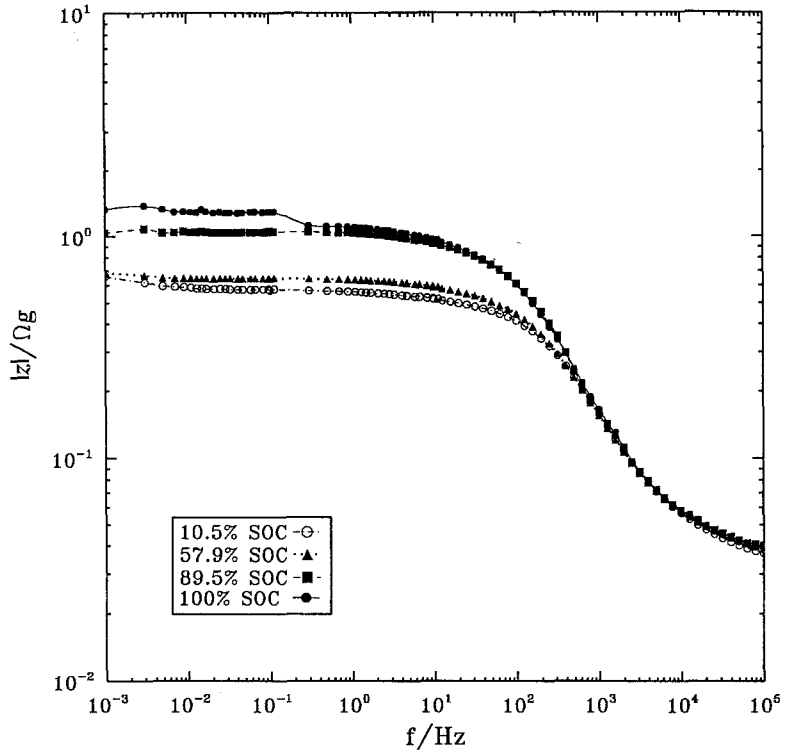

Fig. 6. Typical Bode plots of the electrode. States of charge: (●) 100%, (■) 89.5%, (▲) 57.9% and (○) 10.5%.

Typical linear polarization curves obtained for $La_{0.65}Ce_{0.35}Ni_{3.55}Co_{0.75}Mn_{0.4}Al_{0.3}$ alloy at different states of charge are presented in Fig. 4. If a potentiostatic method were used, the corresponding current would never reach stationary state until the electrode is saturated due to the fact that the hydrogen is adsorbed continuously and because the equilibrium changes with time. However, we carried out linear polarization experiments using the potentiodynamic method which eliminated the problem. Initially, the polarization experiments were carried out at different scan rates (100, 10 and 1 mV s^{-1}). Over this range of scan rates no obvious changes in the polarization curves were observed indicating that the linear polarization curves reached pseudo-stationary state. Therefore, in this study a scan rate of 10 mV s^{-1} was used to carry out the linear polarization experiments.

The exchange current density were estimated using Equation 8 at different states of charge on the electrode and are presented in Fig. 5 as a function of state of charge. As shown in Fig. 5, the exchange current density increases with decreasing the hydrogen content in the alloy and reaches a maximum value at approximately 15% state of charge. Then, the exchange current density starts to decrease with decreasing the hydrogen content in the α phase region of the alloy.

EIS data were obtained with PAR (model 273A) potentiostat/galvanostat and a frequency analyser. Data were stored and analysed using PAR (M398) software on an IBM PC/2. The impedance data generally covered the frequency range from 0.001 Hz to 100 kHz with an a.c. voltage signal varying by ± 5 mV, which ensured the electrode system to be under minimum perturbation. This technique under zero current conditions, enables determination of the polarization resistance and the ohmic resistances (resistance related to alloy particle contact and contact resistance between the current collector and the pellet). Typical Bode plots obtained for different hydrogen contents in the alloy are presented in Fig. 6.

Two equivalent circuits were used in the literature to fit the porous electrode systems [19, 22]. The first equivalent circuit [22] includes a constant phase element (CPE) and is used to describe an approximate straight line behaviour over a limited frequency range. A CPE arises from the presence of inhomogeneities in the electrode system and can be described in terms of a distribution of relaxation times, or it may arise from nonuniform diffusion whose electrical analog is an inhomogeneous distributed RC transmission line [22].

In this study the equivalent circuit of Kuriyama *et al.* [19] was used to fit our EIS data and evaluate the polarization resistance. The fitting was carried out using ZVIEW Software (Scribner Associates, Inc.) which is based on the LEVM 6.0 program written by J. Ross Macdonald.

Calculated polarization resistances using Equation 9 as a function of state of charge in the alloy are presented in Fig. 7. As shown in Fig. 7, the polarization resistance increases with increasing of the hydrogen content in the electrode except at low hydrogen content region. In Fig. 7 the polarization resistances obtained from the EIS data were compared with the data obtained from linear polarization method. Good agreement exist between these two methods when used to estimate the polarization resistance for porous hydride electrode.

To evaluate symmetry factor by using Equation 11, the linear polarization curves in Fig. 4 were replotted accordingly in Fig. 8. From Fig. 8 it can be seen that linear relationships exist between η and $\log i/[\exp(F\eta/RT) - 1]$, and the slopes are 106–

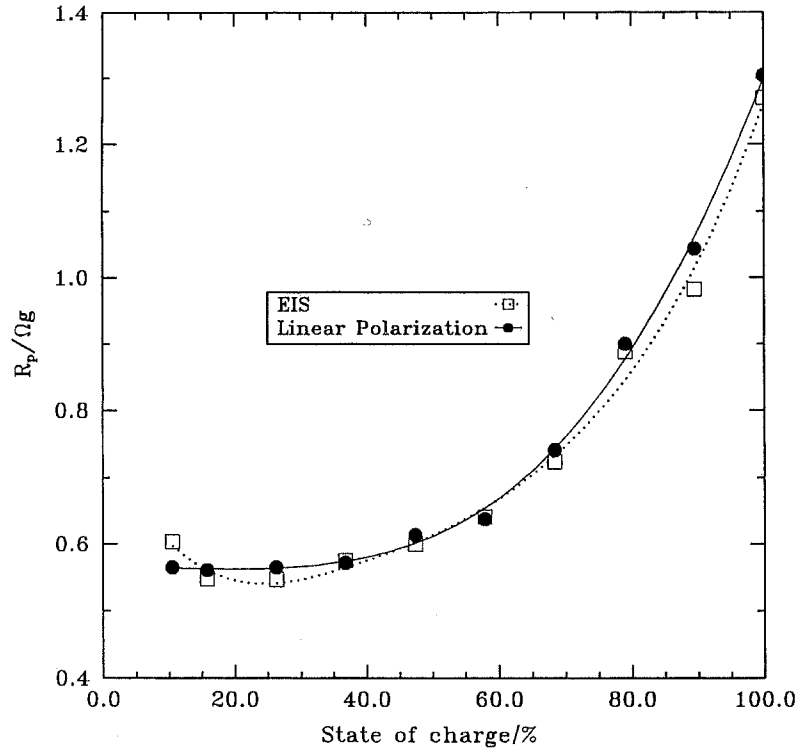

Fig. 7. Polarization resistance of the electrode as a function of state of charge. Key: (●) linear polarization; (□) EIS.

110 mV decade^{-1}. The symmetry factor was evaluated to be 0.55 ± 0.01.

5. Conclusion

Transport and electrochemical properties of $La_{0.65}Ce_{0.35}Ni_{3.55}Co_{0.75}Mn_{0.4}Al_{0.3}$ electrode were investigated in alkaline solution. The exchange current density, polarization resistance and symmetry factor were determined from the polarization curves obtained at low overpotentials. The experimental capacity of the alloy was estimated to be 278 mA h g^{-1} which is about 73% of the theoretical capacity. It was found that as the discharge rate increases, the state of discharge at the end of discharge (cutoff voltage = −0.6 V vs Hg/HgO reference electrode) decreases. This phenomena is due to the depletion of atomic hydrogen from the surface of the M–H particles at high discharge rates which causes the potential to drop before all the hydrogen contained in the particles has been reacted. The charges remaining in the electrode after discharging at different discharging rates were estimated to be 293, 50 and 13 C g^{-1} for discharge rates of 0.5 C, 0.2 C and 0.1 C, respectively. The constant current

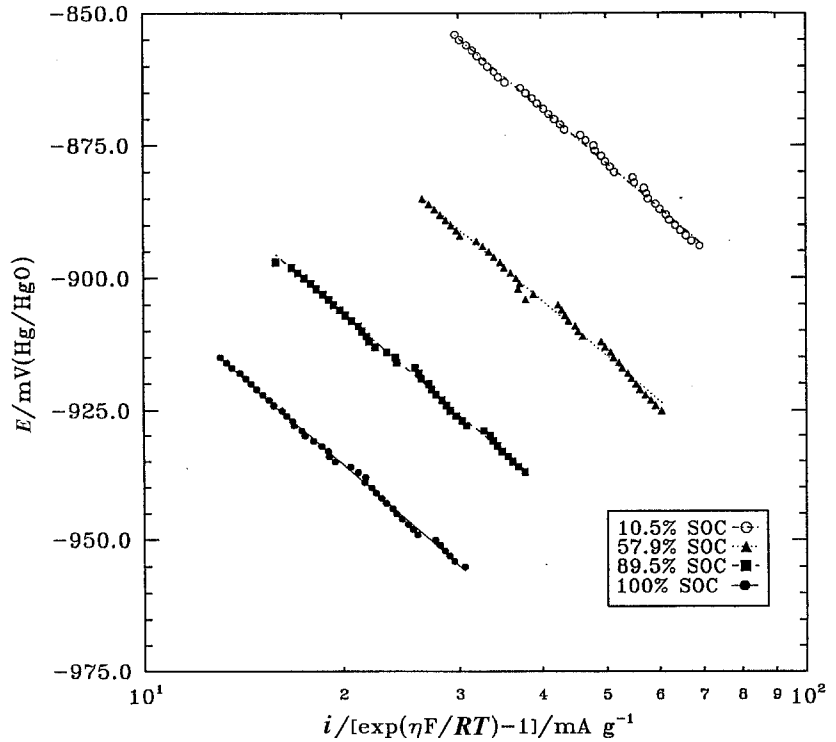

Fig. 8. Dependence of E upon $i/[\exp(\eta F/RT) - 1]$. States of charge: (●) 100%, (■) 89.5%, (▲) 57.9% and (○) 10.5%.

discharge technique was used to determine the hydrogen diffusion coefficient in the alloy. The estimated value of $\tilde{D}/a^2$ at 0.1 C rate was $1.39 \times 10^{-4}\,s^{-1}$. It was found that the equilibrium potential of the electrode depends upon the hydrogen content in the alloy. When the state of charge of the electrode is less than 25% (α phase), the equilibrium potential (−0.903 V vs Hg/HgO reference electrode) shifts in cathodic direction with the increase of the hydrogen content in the alloy. With further increase of the hydrogen content in the electrode, the equilibrium potential reaches a plateau. At this region, two phases α and β (hydride phase) coexist. When only the β phase exists in the alloy (at about 80% state of charge), the equilibrium potential starts to increase again with increase of hydrogen content and at 100% state of charge reaches a value of −0.934 V vs Hg/HgO reference electrode. The polarization resistance, exchange current density and the symmetry factor of the alloy were estimated from polarization curves obtained at low overpotentials. The symmetry factor was estimated to be 0.55 ± 0.01 and is independent of the state of charge.

Acknowledgement

Financial support by the Office of Research and Development under contract 93-F148100-000 is acknowledged gratefully.

References

[1] H. F. Bittner and C. C. Badcock, *J. Electrochem. Soc.* **130** (1983) 193c.
[2] T. Sakai, H. Ishikawa, K. Oguro, C. Iwakura and H. Yoneyama, *ibid.* **134** (1987) 558.
[3] H. Yayama, H. Kuroki, K. Hirakawa and A. Tomokiyo, *J. Appl. Phys. (Japan)* **23** (1984) 1619.
[4] J. J. G. Willems and K. H. J. Buschow, *J. Less-Common Metals* **129** (1987) 13.
[5] A. F. Andersen and A. J. Maeland (eds), 'Hydrides for Battery Storage'. Proceeding of an International Symposium, International Association for Hydrogen Energy, Pergamon, Oxford (1978).
[6] R. Kircheim, E. Fromm and E. Wicke (eds), 'Metal-Hydrides Systems-Fundamentals and Applications'. Proceedings of the First International Symposium combining 'Hydrogen in Metals and Metal Hydrides', Stuttgart, Federal Republic of Germany (1988).
[7] R. Wiswall, 'Hydrogen in Metals II', (edited by Alefeld and J. Volki), Springer-Verlag, Berlin (1978), chapter 5.
[8] H. Yayama, K. Hirakawa and A. Tomokiyo, *J. Appl. Phys. (Japan)* **25** (1986) 739.
[9] P. H. L. Notten and P. Hokkeling, *J. Electrochem. Soc.* **138** (1991) 1877.
[10] L. G. Austin, *Trans. Faraday Soc.* **60** (1964) 1319.
[11] L. G. Austin and H. Lerner, *Electrochim. Acta* **9** (1964) 1469.
[12] T. Sakai, T. Hazama, H. Miyamura, N. Kuriyama, A. Kato and H. Ishikawa, *J. Less-Common Metals* **172** (1990) 1175.
[13] T. Sakai, K. Muta, H. Miyamura, N. Kuriyama and H. Ishikava, *in* Proceedings of the Symposium on 'Hydrogen Storage Materials: Batteries and Electrochemistry', *Electrochem. Soc. Proc.* **92–5** (1992) p. 59.
[14] G. D. Adzic, J. R. Johnson, J. J. Reilly, J. McBreen, S. Mukerjee, M. P. Sridhar Kumar, W. Zhang and S. Srinivasan, *in* Proceedings of the Symposium on 'Hydrogen and Metal Hydride Batteries' (edited by P. D. Bennet and T. Sakai), *Electrochemical Soc. Proc.* **94–27** (1994) p. 24.
[15] P. A. Allen and A. Hickling, *Trans. Faraday Soc.* **53** (1957) 1626.
[16] A. J. Bard and L. R. Faulkner, 'Electrochemical Methods-Fundamentals and Applications', John Wiley & Sons, New York (1980) p. 106.
[17] J. Crank, 'The Mathematics of Diffusion', 2nd edn Clarendon Press, Oxford (1975).
[18] G. Zheng, B. N. Popov and R. E. White, *J. Electrochem. Soc.* **142** (1995) 2695.
[19] N. Kuriyama, T. Sakai, H. Miyamura, I. Uehara and H. Ishikawa, *J. Alloys Comp.* **202** (1993) 183.
[20] G. Zheng, B. N. Popov and R. E. White, *J. Electrochem. Soc.* **143** (1996) 435.
[21] V. M. Lobo, 'Handbook of Electrolytes Solutions', Part A, Elsevier, New York (1989) pp. 1073–1092.
[22] J. R. Macdonald (ed.), 'Impedance Spectroscopy, Emphasizing Solid Materials and Systems', John Wiley & Sons, New York (1987) p. 185.